Space-time pressure structure of pharyngo-esophageal segment during swallowing

ROHAN B. WILLIAMS,[1] ANUPAM PAL,[2] JAMES G. BRASSEUR,[2] AND IAN J. COOK[1]
[1]*Department of Gastroenterology, St. George Hospital and University of New South Wales, Sydney, Australia 2217; and* [2]*Department of Mechanical Engineering, Pennsylvania State University, University Park, Pennsylvania 16802*

Williams, Rohan B., Anupam Pal, James G. Brasseur, and Ian J. Cook. Space-time pressure structure of pharyngo-esophageal segment during swallowing. *Am J Physiol Gastrointest Liver Physiol* 281: G1290–G1300, 2001.—We applied high-resolution manometry with spatiotemporal data interpolation and simultaneous videofluoroscopy to normal pharyngeal swallows to correlate specific features in the space-time intraluminal pressure structure with physiological events and normal deglutitive transsphincteric bolus flow to define normal biomechanical properties of the pharyngo-esophageal (PE) segment. Pressures were recorded by microperfused catheter, and the two-dimensional space-time data sets were plotted as isocontours. On these were superimposed bolus trajectories, anatomic segment movements, and hyo-laryngeal trajectories from concurrent videofluoroscopy. Correlation of the highly reproducible space-time-pressure structure with radiographic images confirmed that primary deglutitive PE segment functions (pressure profile, laryngeal elevation, axial sphincter motion, timing of relaxation, contraction) are accurately discernible from single isocontour pressure visualization. Pressure during bolus flow was highly dependent on axial location within PE segment and time instant. The intrabolus pressure domain, corresponding to the space-time region between bolus head and tail trajectories, demonstrated significant bolus volume dependence. High-resolution manometry accurately, comprehensively, and highly reproducibly depicts the PE segment space-time-pressure structure and specific physiological events related to upper esophageal sphincter opening and transsphincteric flow during normal swallowing. Intrabolus pressure variations are highly dependent on position within the PE segment and time.

bolus transport; deglutition; pharynx; cricopharyngeus; sphincter; fluoroscopy; mechanics; upper esophageal sphincter

THE CRICOPHARYNGEUS is the major muscular component of the upper esophageal sphincter (UES) (12, 29, 41), although controversy remains as to the precise location of the UES high-pressure zone in relation to this muscle (20). The cricopharyngeus muscle has unique biophysical properties suiting it ideally for its functions. It is composed predominantly of type 1 (slow twitch) fibers and has an abundant supply of fibroelastic connective tissue (30). The unique combination of the arrangement of individual muscle fibers and the interstitial fibroelastic tissue accounts for these biophysical properties (5). The cricopharyngeus displays both "passive tension" (i.e., intrinsic or myogenic tone) and "active tension" (extrinsically derived neurogenic tension). For example, with minimal or no neurogenic tone to the sphincter, the cricopharyngeus demonstrates passive tension in the resting state (4, 29). Furthermore, under physiological conditions, the UES has the ability to expand dramatically to accommodate a 20-fold increase in flow rate while offering only minimal increase in resistance (12). Any pathological interference with the compliance of the UES may impair its ability to open fully, thereby increasing the resistance offered by it to bolus flow (13, 15). Under these conditions, there is a marked increase in hypopharyngeal mid-intrabolus pressure, as recorded by a single-point sensor positioned above the UES during flow, which may be normalized by restoring normal UES compliance (40).

Intraluminal manometry, typically in combination with fluoroscopic imaging, is the only method currently available to measure the interplay between UES compliance and the propulsive forces generated by the pharynx to achieve transsphincteric flow during the swallow. High-resolution manometry, used in conjunction with spatiotemporal data interpolation and visualization methods, as, for example, applied to the esophagus (9–11, 26, 31) and stomach (23), has yet to be applied systematically to the pharyngo-UES segment. High-resolution manometry has a significant potential advantage in that a fixed assembly with a sufficient number of closely spaced recording sites can, in principle, capture the basal UES pressure profile, UES pressure relaxation, and the spatiotemporal patterning of pressure changes during individual swallows.

The aims of this study were to apply high-resolution manometry to the pharyngo-esophageal (PE) segment to *1*) correlate specific features in the space-time intraluminal pressure structure with physiological

---

events during the normal swallow; *2*) evaluate the detail in space-time pressure structure during normal deglutitive transsphincteric bolus flow; *3*) use the space-time structure of intraluminal pressure during transsphincteric flow to define the normal biomechanical properties of the muscular components of the PE segment; and *4*) evaluate the intra- and intersubject variability and effect of swallowed bolus volume on these normal biomechanical properties and on the patterning of the space-time pressure structure of the PE segment.

METHODS

Subjects

We studied six healthy subjects (2 male and 4 female) with a mean age of 23 yr (range 21–25 yr) recruited from the community by advertisement. All were screened to ensure that none had swallowing difficulties, medical illnesses, or history of head and neck or gastrointestinal surgery or was taking medications that could have affected swallow function. All subjects gave written informed consent, and the study was approved by the Human Ethics Committees of the University of New South Wales and the South-Eastern Sydney Area Health Service.

Measurement Techniques

Pharyngeal manometry. Manometric data were collected using a custom-designed 11-lumen silicone rubber micromanometric assembly with 10 recording side holes, each spaced at 1-cm intervals and all orientated posteriorly within the pharynx (Dentsleeve, Wayville, Australia). The assembly had an outer diameter of 4.0 mm, and each channel lumen had an internal diameter of 0.4 mm. Radiographic identification of recording sites was achieved by placement of 0.5-mm aluminum markers in the assembly so that the proximal margin of each marker was level with the corresponding side hole. A 5-cm-long section of the assembly between recording *side hole 8* (proximal) and *side hole 3* (distal) was oval in cross section to ensure posterior orientation of all catheter side holes (27). Before intubation and water perfusion, all recording lumina were flushed for a minimum of 5 min with CO_2, which, because of its high solubility in water, ensured removal of microbubbles within the recording lumen and minimized compliance (36). The assembly was then perfused with degassed, distilled water by a low-compliance pneumohydraulic perfusion pump (Dentsleeve) at 0.15 ml/min. The subject was intubated, with the assembly remaining attached to the perfusion pump, after confirmation of water perfusion through all assembly recording lumina. Pressures were registered from each perfused channel by 10 external pressure transducers (Abbott Critical Care Systems, Chicago, IL). Pressure rise rate for this extrusion at the applied perfusion rate is reported by Dentsleeve to be >250 mmHg/s; fall rates are more rapid than rise rates. Signals were collected using a computer-based data acquisition system (MP100, BIOPAC Systems, Santa Barbara, CA, with Acqknowledge v3.1.2) running on an Apple IIci Macintosh computer. Unless otherwise stated all signals were acquired at a sampling frequency of 200 Hz per channel.

Combined videoradiography. Swallows were recorded by simultaneous videoradiography and manometry as described in detail previously (3, 12). Briefly, swallows were recorded in lateral and anteroposterior projections using a 9-in. Toshiba (Kawasaki, Japan) image intensifier, and images were recorded on video tape at 25 frames/s by a VHS video recorder (AG6500; Panasonic, Osaka, Japan) for later analysis. The correction factor for magnification was determined before each study by placing two metallic markers set 3 cm apart in the field of the image intensifier, above the subject's head but in the plane of the UES. Subjects swallowed duplicate 2-, 5-, 10-, and 20-ml boluses of liquid barium suspension [250% wt/vol, density 1.8 g/ml (32), E-Z-HD; E-Z EM, Westbury, NY]. Included in the field of view in the lateral projection were the incisor teeth anteriorly, hard palate superiorly, cervical spine posteriorly, and proximal cervical esophagus inferiorly. Fluoroscopic flaring was reduced by having the subject hold a water-filled latex glove loosely against the skin under the chin. A video digital timer (Practel Sales International, Holden Hill, Australia) simultaneously imprinted the elapsed time on the video images (in hundredths of seconds) and a timer signal onto the manometric trace, thus permitting precise temporal correlation between fluoroscopy images and manometric data.

Experimental Protocol

After a fasting period of at least 4 h, the manometric catheter was passed transnasally into the esophagus and was withdrawn stepwise until the recording sites corresponding to the ovalized section of the catheter straddled the UES high-pressure zone. In this position, the three most proximal side holes lay within the pharynx. After a 10-min adaptation period, basal UES pressure was measured. Subjects then swallowed duplicate volumes of liquid barium (2, 5, 10, 20 ml) recorded with concurrent videofluoroscopy (see *Combined videoradiography*). The recording assembly was perfused only during the period of the swallow recording to minimize pharyngeal stimulation by perfusate. Total fluoroscopic exposure time was <2 min.
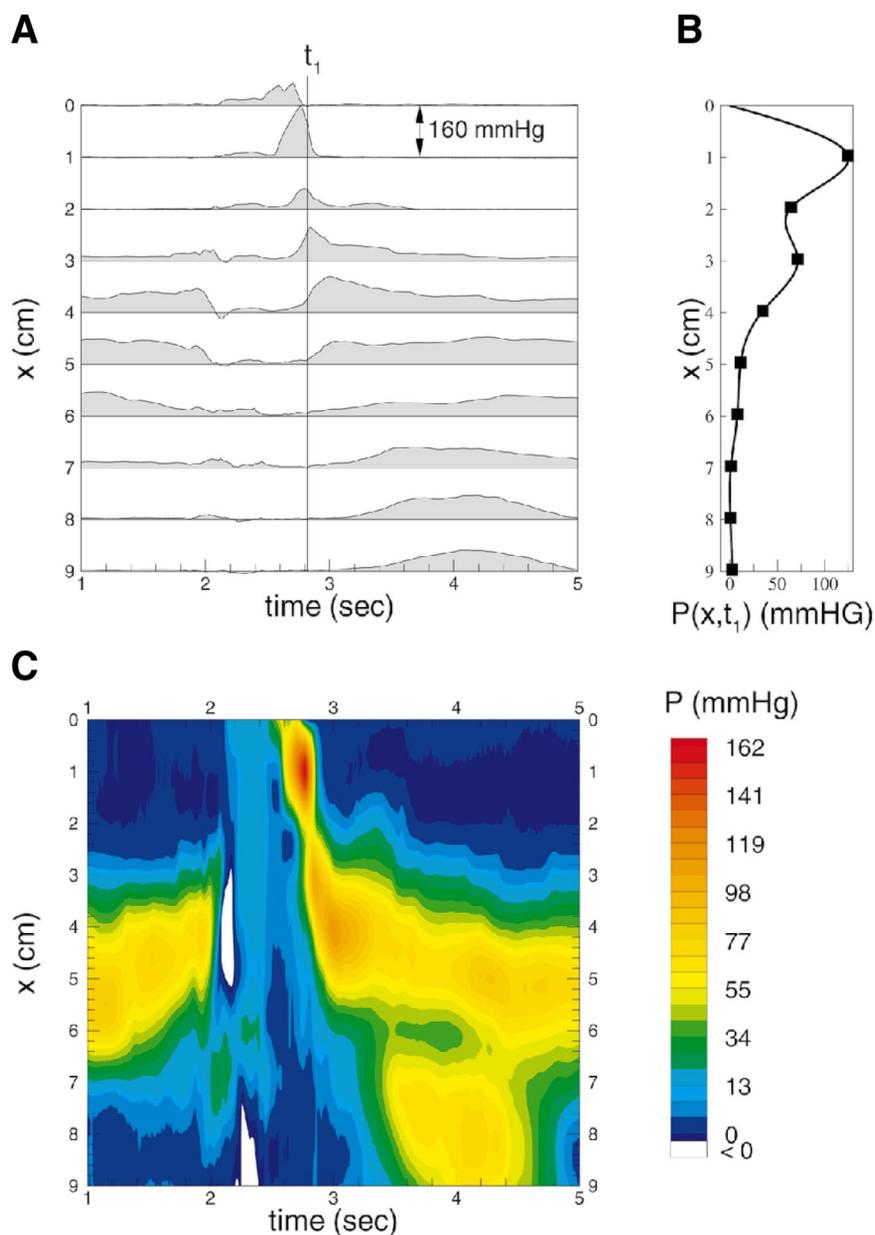
Data Analysis and Definitions

Preprocessing of manometric data. Pressures recorded at each channel were first corrected for differences in perfusion and hydrostatic offsets among recording channels (36) by subtracting pressure offsets measured relative to an arbitrary reference side hole while the catheter was perfused in the vertical orientation external to the subject. All pressures were referenced to resting hypopharyngeal (atmospheric) pressure.

To improve the spatial representation of pressure axially through the PE segment, pressures were interpolated between the values obtained at each individual 1-cm-spaced recording site from the hypopharynx through to the cervical esophagus using cubic-spline interpolation (38) at each time instant. In this way, 30 "virtual" pressure values were generated between each of the 10 recording sites (Fig. 1*B*). The resulting spatiotemporal pressure data were displayed in three related formats: *1*) temporal variation in pressure displayed at several fixed spatial locations (traditional or "strip chart" representation of Fig. 1*A*); *2*) spatiotemporal variation in pressure plotted as lines of constant pressure, shown as bands of constant color, as a function of distance along the lumen and time ("isocontour" representation of Fig. 1*C*); and *3*) spatial variation in pressure as an axial plot through the PE segment at fixed time instants *("spatial"* representation, Fig. 2, *A–F*).

A fundamental characteristic of initial phases of bolus transport is the highly time-dependent nature of the process, raising the question of which time instant, or time period, is most appropriate for measurement of transsphincteric intrabolus pressure. We found that during the transsphincteric flow period the flow, and corresponding spatial pressure

Fig. 1. Defining the space-time pressure structure from multichannel manometric data. *A*: manometric recording of a 5-ml barium swallow in healthy control. Pressure is interpolated along vertical lines at fixed times using cubic splines. *B*: an example interpolation [P(*x*,*t*), variation of pressure with spatial localization, *x*, at time instant, t_1] at *time* t_1 shown by the vertical line in *A*. The interpolation procedure is repeated at each time instant in the data record and results in a 2-dimensional, spatiotemporal distribution of pressure data. This 2-dimensional pressure distribution is displayed in *C* with bands of color representing different pressure levels as a function of spatial location (vertical axis) on the catheter axis and time (horizontal axis). The white contour denotes subatmospheric pressure. Distances on vertical axis are referenced to the most proximal recording site, which is positioned in the hypopharynx. Note the clearly discernible high-pressure zone before and after the swallow, which is abolished for ~800 ms during deglutitive relaxation and the passage of the bolus. The pharyngeal propagating pressure wave (rapid transition to yellow/red region starting at 2.5 s at 0.0 cm), resulting from contraction of the pharyngeal walls, is clearly observed to propagate inferiorly through the pharynx and into the upper esophageal sphincter (UES) region, closing the UES and reestablishing the resting sphincteric high-pressure zone (*t* > 3.5–4 s). Interestingly, a short delay in propagation is observed at the distal margin of the UES (*t* = 2.8 s, at ~6 cm), before the initiation of the propagating pressure waveform in the cervical esophagus (starting at *t* = 3.0–3.1 s and ~6.0 cm). By roughly *t* = 5 s, the pharyngo-esophageal (PE) segment has returned to resting state.

distribution through the UES, attain a period of relatively slow change in time—a "quasi-steady" period of transsphincteric flow (see RESULTS). To quantify axial pressure variation through the UES during this quasi-steady period, a 150-ms window was extracted beginning 100 ms after the entry of the bolus head into the UES segment (Fig. 2, *A* and *B*), and over this period the pressure was averaged in time at each virtual port along the catheter.

Correlation of fluoroscopic images with manometry and intrabolus domain. Fluoroscopic images were digitized from videotape and imported into a graphics workstation (SGI Indigo; Silicon Graphics, Palo Alto, CA) and were displayed and analyzed using custom-designed software written in MATLAB 5.1 (Mathworks, Natick, MA). We determined manually the *x-y* coordinates of the locations of five features from each of the images: *1*) bolus head, *2*) bolus tail, *3*) posteroinferior margin of the vocal cords [i.e., posterosuperior corner of the tracheal air column (12)], *4*) anteroinferior aspect of the hyoid bone, and *5*) anteroinferior corner of the

C3 vertebra. Calibration of distances was achieved from the known distance between side hole markers.

To delineate the space-time periods that corresponded to transsphincteric bolus flow, we plotted the trajectories of the bolus head and bolus tail on the isocontour plot of space-time pressure structure during individual swallows. The spatial axis of the isocontour plot corresponds to the location of the recording side holes along the catheter, with the location of the most proximal side hole corresponding to 0.0 cm on the spatial axis of pressure. We defined a curvilinear coordinate system along the side hole markers, referenced to the location of the most proximal marker, on which the location of the bolus head and tail were projected to obtain their corresponding locations on the curved spatial axis. Because of catheter motion associated with laryngeal elevation (24, 28), the catheter coordinate system was updated in each frame before the arrival of the bolus head at the most proximal side hole. We defined the intrabolus pressure domain as the region of the isocontour plot bounded by the bolus head and tail trajecto-
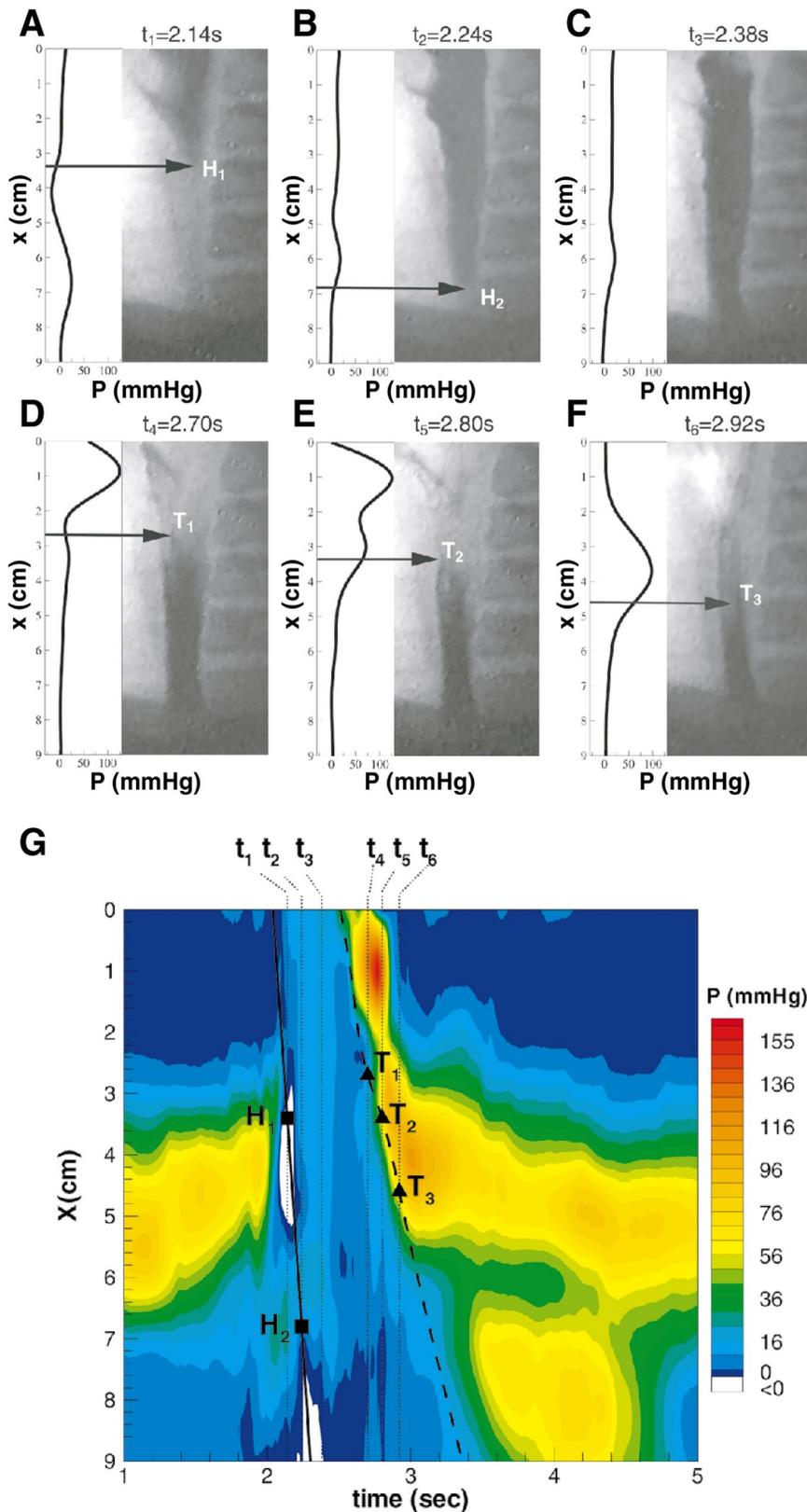
Fig. 2. Correlation of videomanometric events with space-time pressure history (5-ml bolus). A–F: composite of 6 radiographs taken at various times (t_1–t_6) across the swallow sequence shown in Fig 1. The axial pressure structure through the PE segment at each time instant is shown next to each radiograph. Spatial locations of the advancing swallowed bolus head (H_1 and H_2) and tail (T_1–T_3) on each axial pressure plot and corresponding radiograph are indicated by right-facing arrows. The space-time locations of the bolus head and tail are presented on the space-time pressure history plot (G). Passage of the bolus head through the hypopharynx correlates closely with a low-amplitude step increase in hypopharyngeal pressure seen as a transition from darker to lighter blue isocontours at $\sim t = 2$ s between 0 and 2.5 cm. Hence, the interval between bolus head and tail trajectories defines the intrabolus pressure domain. The arrival of the bolus head (H_1) into the sphincter zone is coincident with the transient subatmospheric drop in UES pressure illustrated by the pressure trace in A and the white isocontour section in G. The quasi-steady state within the intrabolus pressure domain is represented by interval between t_2 and t_3 (see text). Panel G shows the very close temporal relationship between the trajectory of the bolus tail (T_1–T_3) and the time-dependent, rapid transition in pressures throughout the UES demonstrated by color shift from blue to orange. The head trajectory curves proximal to H_1 and distal to H_2 are linear extrapolations from the H_1–H_2 segment. The tail trajectories are linearly extrapolated proximal to an unplotted point at 2 cm and distal to T_3.

ries (see isocontour representation in Fig. 2G). The location of the resting UES high-pressure zone was referenced to the resting position of the posterosuperior corner of the tracheal air column.

The superior and anterior motion of the hyoid bone and larynx during swallowing were plotted relative to the catheter orientation with the C3 vertebra as the zero reference. Superior-inferior motions were defined parallel to the cathe-

A

$P^{(1)}(x,t)$

B

$t_{r1}^{(1)}$ $t_{r2}^{(1)}$

mim pressure drop   max pressure rise

C

Normalized pressure $\hat{P}^{(1)}$

$P^{(2)}(x,t)$

$t_{r1}^{(2)}$ $t_{r2}^{(2)}$

min pressure drop   max pressure rise
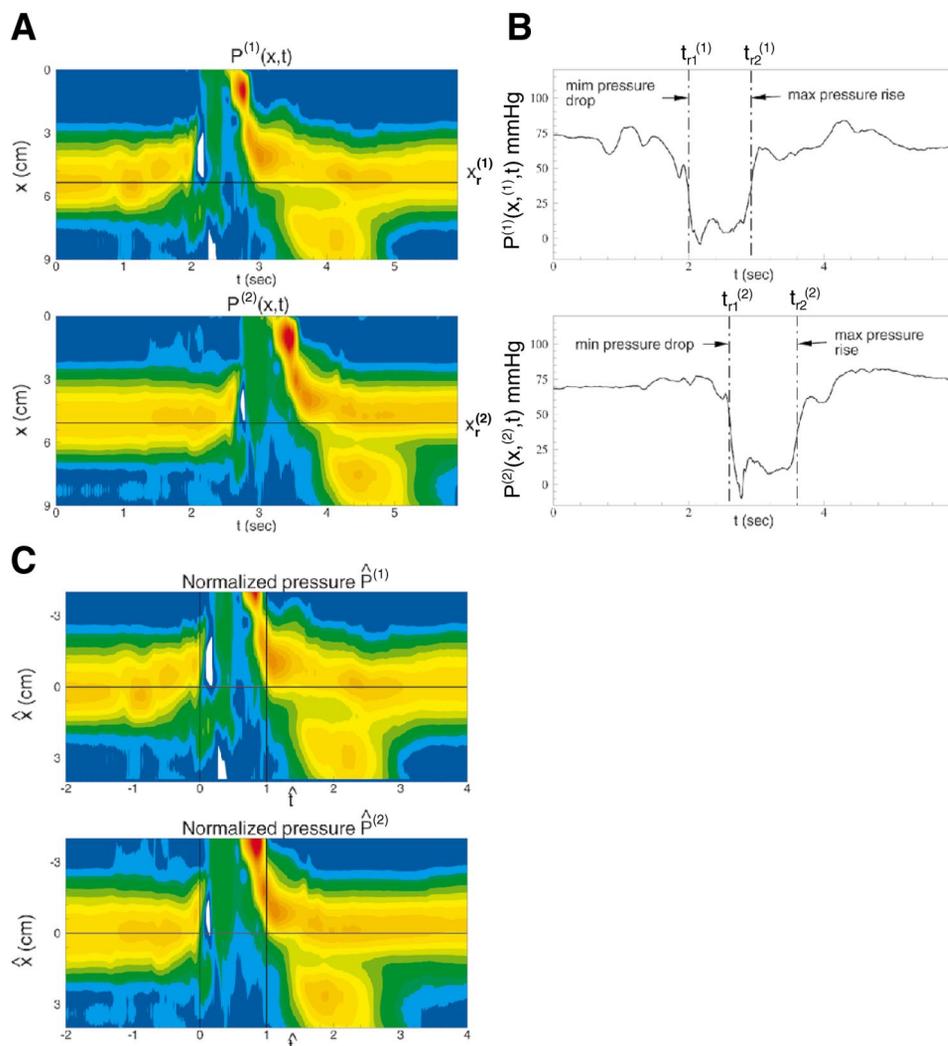
Normalized pressure $\hat{P}^{(2)}$

Fig. 3. Methodology for constructing ensemble averages of space-time pressure representations of swallow data by aligning swallows spatially and temporally (see METHODS). *A*: the spatial reference (horizontal lines marked $x_r^{(1)}$, $x_r^{(2)}$) is the axial position of maximum preswallow UES pressure. *B*: the 2 time reference points are the points of maximum negative (t_1) and maximum positive (t_2) pressure-time gradients at x_r (see text); t_1 occurs during relaxation and opening, and t_2 occurs during the passage of the bolus tail and closure of the sphincter. With the use of these 3 reference points, the swallows were aligned in space and time (*C*) and averaged to produce the final ensemble average.

ter axis, whereas anterior-posterior motions were defined perpendicular to the catheter axis.

Ensemble averaging of space-time pressure data. To evaluate features common to most normal swallows, we calculated ensemble average space-time pressure distributions within bolus volume groups appropriately normalized. In this way, the more stereotypical features were enhanced while highly variable features (noise) were suppressed. We evaluated ensemble-averaged pressures to determine the extent to which detailed variations in space-time pressure structure could be correlated with bolus transport and intraluminal geometry.

To extract pressure features associated with transsphincteric flow it was necessary to align and normalize the space-time pressure structure to account for the bolus volume-dependent increases in UES opening time. Images were aligned both temporally and axially by first estimating temporal and spatial reference points and then overlaying each isocontour representation for each consecutive swallow anchored by their common temporal and spatial reference points (Fig. 3). The spatial reference point in each swallow (x_r) was defined as the location of maximum pressure in the preswallow resting UES high-pressure zone, calculated over a 250-ms time window (see Fig. 3*A*). We normalized the time axis relative to the transsphincteric flow period by choosing two temporal reference points extracted from the space-time

pressure data at spatial reference point x_r. As shown in Fig. 3*B*, the first temporal reference point (t_{r1}) corresponds to the minimum (negative) temporal pressure gradient occurring during the rapid intrasphincteric pressure drop just before UES opening. The second temporal reference point (t_{r2}) corresponds to the maximum (positive) temporal pressure gradient occurring during the short period of rapid rise in intrasphincteric pressure created by the passage of the pharyngeal stripping wave through the PE segment, closing the segment (Fig. 3*B*). The temporal pressure gradient is given mathematically by the derivative of pressure with respect to time, $\partial P(x_r,t)/\partial t$. Thus the minimum (negative) temporal pressure gradient and the maximum (positive) temporal pressure gradients are given by $[\partial P(x_r,t)/\partial t]_{min}$ and $[\partial P(x_r,t)/\partial t]_{max}$, respectively. These gradients were calculated using a numerical differentiation scheme that was smoothed before calculation of t_{r1} and t_{r2} with a low-pass filter.

The pressure data were aligned spatially with respect to the spatial reference point x_r, and the midpoint of the UES high-pressure zone was defined as 0 cm. The pressure data were then temporally normalized between the two reference times such that, for each component swallow, the first temporal reference time t_{r1} was defined as 0.0 and the second temporal reference time t_{r2} was defined as 1.0. Pressure data before t_{r1} and after t_{r2} were aligned to match these temporal

references. The aligned and normalized pressure are given mathematically by

$$\hat{P} = P(\hat{x},\hat{t})$$

where

$$\hat{x} = x - x_r$$

$$\hat{t} = (t - t_{r1})/\Delta t$$

$$\Delta t = t_{r2} - t_{r1}$$

Fig. 3*C* shows the result of the normalization procedure applied to the two example swallows shown in Fig. 3*B*. Once data from all component swallows were aligned and normalized, we calculated the ensemble average pressure

$$\langle \hat{P}(\hat{x},\hat{t}) \rangle = \frac{1}{N}\sum_{k=1}^{N} P_k(\hat{x},\hat{t})$$

where N is the number of individual swallows.

The temporal normalizations obtained as described above from the manometry data were also applied to the trajectories of the bolus head and tail obtained from the images so that average head and tail trajectories obtained fluoroscopically could be correlated with the ensemble-averaged space-time pressure structure obtained manometrically.

Statistics. Statistical inferences regarding the effect of bolus volume on spatial pressure variation measured during the intrabolus pressure domain were made using a repeated-measure ANOVA model (14). Spatial location was treated as the repeated-measure variable. Because of the large number of data samples in each spatial pressure variation data series, prior data reduction was achieved by first averaging values over 1-cm intervals. An α (P) value <0.05 was considered to indicate statistical significance. Data are presented as means ± SE unless stated otherwise.

RESULTS

Spatial Representation of UES High-Pressure Zone at Rest

The axial pressure profile and position of peak pressure in the resting UES high-pressure zone varied quite markedly among subjects (Fig. 4). The mean distance between peak resting UES pressure and the inferior margin of the vocal cords was 1.9 ± 0.4 cm (range 0.5–3.3 cm). The mean maximum resting UES pressure was 84 ± 13 mmHg (range 56–127 mmHg). The axial length of the high-pressure zone corresponding to 50% of maximal pressure averaged 2.1 ± 0.3 cm (range 1.4–2.9 cm) (Fig. 4). Five of six subjects showed a transient prerelaxation augmentation in UES pressure at the distal margin of the UES (e.g., 7 cm at 1.9 s; Fig. 1*A*).

Interpretation of Space-Time Pressure Structure During Swallow

Figure 1*B* shows an isocontour representation of the space-time pressure structure of a 5-ml barium swallow and a comparison with the strip chart representation in Fig. 1*A*. Before the initiation of the swallow ($t <$ 1 s), the UES is closed and at rest and the sphincteric high-pressure zone is clearly discernible as a horizontal band of yellow and red delineating higher pressure
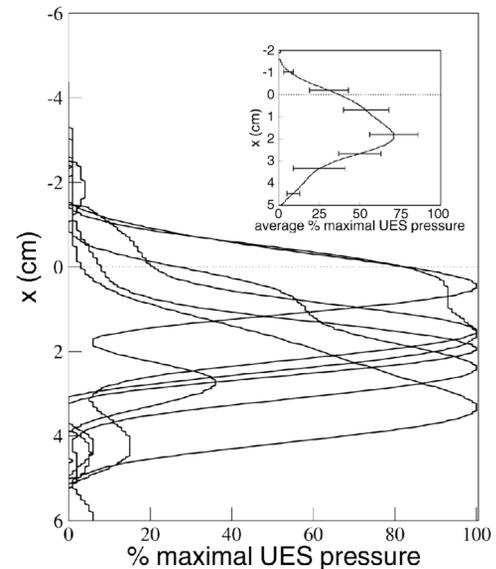

Fig. 4. Spatial (axial) distribution of resting pressure across the PE segment shown for the 6 subjects. Pressure is expressed as a percentage of the individual maximal pressure recorded across the high-pressure zone. Zero denotes the resting location of the postero-superior corner of the tracheal air column, corresponding to the undersurface of the true vocal cords. Note that the location of peak pressure varies greatly among subjects. The proximal and distal margins of the UES high-pressure zone clearly extend beyond the predicted upper and lower margins of the cricoid cartilage, confirming that inferior pharyngeal constrictor and cervical esophageal muscle fibers contribute to resting UES pressure. *Inset*, group mean resting UES pressure. The mean peak pressure location occurs at ~1.9 cm distal to the level of the undersurface of the true vocal cords.

relative to both pharyngeal and cervical esophageal pressures. In this individual, the resting high-pressure zone is ~4cm in width.

The initiation of the swallow is evident at ~1.2 s as the isocontours in the UES high-pressure zone begin to shift superiorly before a rapid reduction in pressure. The high-pressure zone begins to reestablish its resting position again at completion of the UES relaxation phase, reaching its original position at roughly 3.4 s. Hence, the superior/inferior shift spans roughly 2.2 s. As shown in *Average Space-Time Pressure Pattern*, this superior/inferior shift of isocontours reflects the relative motion between the catheter and UES during laryngeal elevation.

The initial superior excursion of the high-pressure isocontours is followed by an abrupt drop in pressure, in some cases to subatmospheric levels, which is depicted by a vertically oriented transition from yellow-orange to green/blue at ~1.8 s between 2.5 cm and 6 cm. This corresponds with UES relaxation and sphincter opening (Figs. 1 and 2). The brief (50 ms) drop to subatmospheric pressures was observed consistently in two of the six subjects. In Fig. 1*B*, this subatmospheric pressure drop is identified by the white region extending axially from ~3.25 cm to 5 cm at ~ 1.9 s. The initiation of the subatmospheric pressure transient was seen to coincide with the rapid separation of the posterior and anterior walls of the sphincter zone (Ref. 22; the instant shown in Fig. 2*A*, t = 2.14 s). The

propagating pharyngeal pressure wave arrives at the UES coincident with reestablishment of UES tone at the completion of the relaxation phase and transsphincteric flow (Fig. 2D; $t = 2.7$ s). After passing through and closing the UES, the contraction wave momentarily decreases in amplitude before establishing the cervical esophageal peristaltic wave.

Correlation of Bolus Trajectory With Space-Time Pressure Structure

Superimposition of the bolus head and tail trajectories onto the isocontour pressure plot shows that passage of the bolus tail correlated closely with the onset of the upstroke of the pharyngeal pressure wave as it propagated distally through the PE segment (Fig. 2G; transition from green to yellow contours along propagating pressure wave). Passage of the bolus head through the hypopharynx correlated closely with a low-amplitude step increase in hypopharyngeal pressure (Fig. 2G). This increase in pressure signals the initiation of what is commonly referred to as the "ramp" or hypopharyngeal intrabolus pressure domain that precedes the propagating pharyngeal contraction wave. The bolus head enters the UES at a velocity of 42 cm/s during the period of the subatmospheric pressure drop, raising intrasphincteric pressure as the opened UES region fills with bolus. Hence, the trajectory of the bolus head correlates closely with the nadir pressure over the axial length of the UES (Fig. 2).

Individual curves of spatial variation in pressure at different times marked on the isocontour plot are shown in Fig. 2, A–F. Time $t_1 = 2.14$ s (Fig. 2A) occurs just at the time of UES opening, where a momentary drop to subatmospheric pressures is observed over the segment from 3 to 5 cm ("zero" pressure in all figures is atmospheric). Pressure rapidly recovers to atmospheric along the PE segment as the bolus enters the UES (Fig. 2B) during the period of UES opening (Fig. 2, A–C). As the stripping wave is established in the hypopharynx (Fig. 2D), pressure is observed to drop continuously from the upper to lower UES (Fig. 2, D, E, and distal end of F), and this pattern remains relatively constant in time until the contraction wave and bolus tail move through the PE segment (Fig. 2, D–F). With the passage of the stripping wave through the UES, the segment closes and UES pressure increases, initially to values above resting-state pressure but later to resting-state values as esophageal peristalsis is established (isocontour plot, Fig. 2G).

Average Space-Time Pressure Pattern

Figure 5C shows the ensemble average of the isocontour representation on which is superposed the ensemble average of the bolus head and tail trajectories for the 5-ml group (Fig. 5, A and B, showing laryngo-hyoid trajectory data, are discussed in *Correlation of Larnygo-Hyoid Motion With Space-Time Pressure Structure*). As in the example of the single swallow above, in the ensemble average the correlation between the bolus head and tail trajectories and features in the space-
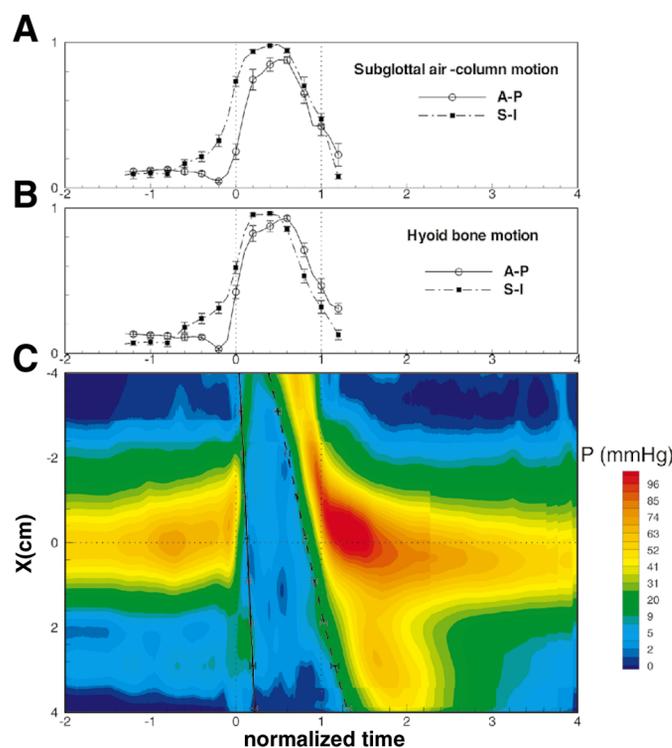

Fig. 5. Ensemble average plot showing group average space-time pressure history for 5-ml boluses; superimposed bolus head and tail trajectories (C) and larnygo-hyoid motion (A and B). Note that the trajectories have been normalized and the time scales in A–C are identical (see METHODS). The correlation between the bolus head and tail trajectories and features in the space-time pressure structure were highly reproducible in the average isocontour representation from all subjects. Note the close temporal relationship between the passage of the bolus head into the UES and the minimum intrasphincteric pressure shortly after UES opening and between the passage of the bolus tail and the upstroke in the propagating pharyngo-UES pressure wave. Note also that intrabolus pressure decreases axially across the opened UES at all time instants on average.

time pressure structure were highly reproducible in the average isocontour representation from all subjects. In particular, highly stereotypical temporal relationships are observed between *1*) the bolus head trajectory and the onset of the hypopharyngeal intrabolus (ramp) pressure domain, *2*) the passage of the bolus head into the UES and the minimum intrasphincteric pressure shortly after UES opening, and *3*) the passage of the bolus tail and the upstroke in the propagating pharyngo-UES pressure wave. As in the individual minimum ensemble average, intraluminal pressure that occurs just after UES relaxation onset does not become subatmospheric because only two of the six subjects had consistent subatmospheric pressure drops.

The ensemble-averaged pressure during transsphincteric flow was highly dependent on both the axial location within the PE segment and the particular time instant during the period of transsphincteric bolus flow. The changes in color demonstrate that intrabolus pressure decreases axially across the opened UES at all time instants on average (Fig. 5C). The

magnitude and other details of this spatial drop in pressure vary with time; however, the time rate of change in this spatial pressure structure is greater during the earlier phase of transsphincteric flow, immediately after the passage of the bolus head, than toward the later period of transsphincteric flow before the arrival of the pharyngeal pressure wave.

Spatial Variation in Intrabolus Pressure Across PE Segment

We evaluate the transsphincteric intrabolus pressure gradient during the quasi-steady period, a 150-ms time window beginning 100 ms after the initial entry of the bolus head into the UES segment (see *Data Analysis and Definitions*). In Fig. 2, this corresponds approximately to the period from *panel B* to *panel C*. Figure 6 shows the resulting time-averaged spatial pressure distribution subsequently ensemble-averaged within volume groups. Intrabolus pressure always decreased inferiorly across the UES but with a volume-dependant increase in the gradient or slope of pressure drop across the PE segment during trans-UES bolus flow. The bolus-dependent differences in intrabolus pressure were greatest in the hypopharyngeal and proximal UES (x between -3 and 0 cm; $P < 0.05$ with repeated-measures ANOVA). The same volume dependence in hypopharyngeal pressure from single-point measurements was shown previously (12). In the distal UES region, however, intrabolus pressure is much less sensitive to bolus volume (the difference in pressure in the region $x \approx 0$–3 cm is not statistically significant). Because the average of the pressure gradient equals the gradient of the average pressure, we conclude that there is an overall increase in pressure gradient magnitude with bolus volume.
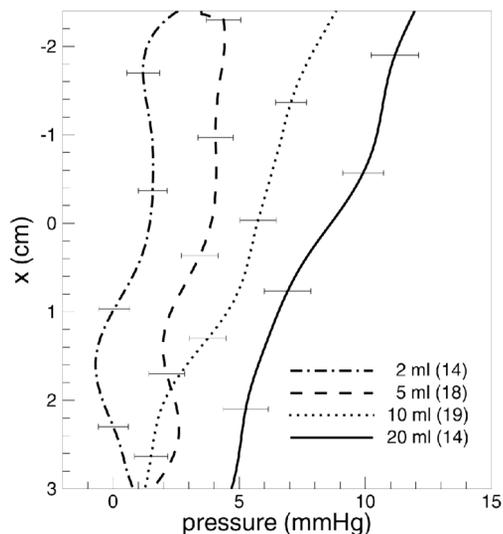

Fig. 6. Spatial pressure distribution within the intrabolus pressure domain. Data shown are averaged values obtained during the quasi-steady-state region of this domain (see text). The axial location of the maximum resting UES pressure is designated as 0 cm on the vertical axis. Note the effect of swallowed bolus volume on the spatial distribution of intrabolus pressure.

Correlation of Larnygo-Hyoid Motion With Space-Time Pressure Structure

The ensemble-averaged superior and anterior excursions of the larynx and hyoid bone in Fig. 5, *A* and *B*, are compared directly with the ensemble-averaged space-time pressure structure of Fig. 5*C*. Consistent with previous studies, the superior laryngeal and hyoid motions precede their anterior motions and anterior excursion of both straddles the relaxation onset and initial opening phases of the UES (12, 25). It is also noted that the ensemble-averaged isocontours shift superiorly before UES opening and transsphincteric flow and then inferiorly after UES closure, in close correlation with the superior-inferior motions of the larynx and hyoid bone (Fig. 5). It is important to note that UES opening, which occurs between the time zero and tail trajectory lines drawn in Fig. 5*C*, occurs while the hyoid bone is in mid-anterior excursion, but the larynx is much earlier in its anterior excursion on average.

DISCUSSION

Using high-resolution manometry we have measured the changes in pressure concurrently in time and along the lumen that result from the space-time changes in muscle squeeze, anatomy, and intrabolus pressure forces generated at rest and during the transport of liquid boluses through the PE segment in healthy humans. From a single space-time data representation using isocontours the interrelationships between temporal and spatial changes in pressure throughout entire swallows are readily apparent. We have related, with a high degree of precision, specific spatiotemporal pressure patterns from the isocontour plots to specific muscular actions, radiographic features, and bolus transport events. The reproducibility of these relationships during the normal liquid bolus swallow is sufficient to confidently predict the initiation and completion of the pharyngo-UES phase of the swallow, the opening and closure of the UES, and the timing of bolus flow from the isocontour plots alone. Importantly, this study provides a detailed spatial distribution of intrabolus pressure across the PE segment for the entire duration of transsphincteric flow.

Hypopharyngeal intrabolus pressure has been applied to estimate the resistance to bolus flow through the UES during transsphincteric bolus flow (13, 15, 25, 33) and might be a useful predictor of postmyotomy outcome (2, 34, 40) or as a pointer for other therapy (19, 39). However, because hypopharygneal mid-intrabolus pressure is measured at a single spatial location proximal to the sphincter at a single point in time, it can only suggest, indirectly, the dynamics of UES function, which in reality, as we have shown, varies rapidly in time and space during UES opening and transsphincteric flow. Newton's second law of mechanics would indicate that the forces that drive the bolus through the sphincter are given not by pressure per se but rather by pressure gradient (the slope in the pressure vs. distance curve), a quantity that, like pressure,

varies rapidly in space and time during UES opening and bolus flow. Newton's law indicates that the intrabolus pressure gradient reflects both the acceleration/deceleration of the bolus flow and the frictional resistance to flow (6). The space-time variation in pressure and the pressure gradient throughout the PE segment during a swallow should provide more relevant information on the physiology of a swallow than can be obtained through a single pressure measurement proximal to the UES at a single point in time, as measured traditionally.

The current study demonstrates the dynamics of UES opening/closure and transsphincteric bolus flow in relationship to the time evolution of the axial pressure distribution (Fig. 2), indicating a close coupling between UES opening and a rapid drop in pressure through the UES segment, often to subatmospheric pressure. We averaged the spatial structure of pressure over time during quasi-steady periods of bolus flow less affected by the rapid transients associated with UES opening and closure to obtain a single representative pressure gradient (Fig. 6). These average pressure curves indicate a sensitivity between intrabolus pressure gradient and bolus volume that reflects an increased UES resistance to flow segment at larger bolus volumes.

Spatiotemporal interpolation of manometry represented with multiple visual modalities to bring out both spatial and temporal variations in pressure during pharyngeal-UES-esophageal transport yields most details of space-time pressure structure so long as the spatial resolution of the point sensors is sufficiently high to capture the spatial variations of interest (9–11, 23, 26). Interpolated space-time pressure represented with isocontours, in particular, presents in one image the spatial and temporal structure of muscle squeeze changes along the PE segment over the period of the swallow, allowing for rapid interpretation. Supplemented with line plots of the spatial variation in pressure along the lumen at multiple time instants and temporal variations in pressure at multiple spatial locations, sufficiently well-resolved manometry can provide detail with potentially important interpretative value. Because the major pressure component of the UES is ~1 cm in width (12), a spacing of at least 1 cm between manometric ports is necessary to capture the spatial pressure structure within it. Currently, a resolution of ≤1 cm is only achievable with microperfusion manometry. The advantage of perfusion manometry is its versatility and the extremely high spatial resolution that is achievable (11, 23, 26). Although peak pharyngeal contraction pressures are likely to be underestimated by perfusion manometry (18, 37), we show in this study that the assembly (rise rate of 250 mmHg) has sufficiently low compliance to capture the primary elements of pharyngo-UES dynamics while faithfully recording the rapid drop to subatmospheric pressure accompanying UES opening and details of the intrabolus pressure domain (Figs. 1 and 2). The techniques described in this study could be applied equally well to solid state manometry, which has a higher frequency response, if the practical barriers of cost and limitations of transducer proximity could be overcome.

The technique is particularly valuable in its ability to accommodate the well-recognized relative deglutitive axial motion of the UES on the catheter (24, 28). The technique allows, for example, determination of the initiation of laryngeal elevation before UES opening and return to resting position after UES closure (Figs. 1, 2, and 5) and the precise timing and completeness of UES relaxation. Although pressure recordings made from the sleeve sensor (16, 27) and derivative solid-state devices (7) can also accommodate axial motion of the UES during swallowing, they cannot resolve the extent or timing of such motion. Furthermore, a sleeve sensor records only the maximum pressure along its length but no details of the space-time-pressure structure within the UES during flow. In contrast, high-resolution manometry can provide a precise representation of the axial distribution of pressure from which both superior motion and duration of UES relaxation can be obtained, both of which are difficult to determine with a sleeve or single-point sensors (1, 17, 28). As shown in the present study, the duration of UES relaxation and UES opening period at any level of the UES region and axially dependent variations in the duration of relaxation that result from greater superior motion of the sphincter than the manometric catheter are readily obtained (Figs. 1, 2, and 5).

Using ensemble averaging we found that intra- and intersubject variability from the stereotypical pattern of space-time pressure-flow dynamics during pharyngo-UES transport is remarkably minimal (Fig. 5). This observation suggests a high level of homogeneity within the medullary pattern generator, translating into similarity of spatiotemporal pressure patterning among healthy subjects for a given bolus volume.

With this technique the basal profile of the UES high-pressure zone can be assessed without combined fluoroscopy and manometry and a pull-through that itself may stimulate muscle contraction and spuriously elevate UES pressure (17). Group mean UES pressure profile data (Fig. 4, *inset*) put the high-pressure zone midpoint 1.9 cm distal to the undersurface of the vocal cords, comparable with previous studies (12, 28, 35, 41). However, the individual resting UES pressure profiles reveal marked variability in the location, length, and structure of the UES resting high-pressure zone, consistent with the study by Nilsson et al. (35). Because the posterior lamina of the cricoid cartilage is 2.5–3 cm in length with its proximal margin 4–8 mm above the undersurface of the vocal cords (42), the results from Fig. 4 imply that the high-pressure zone extends above and below the cricoid cartilage, consistent with the probable contribution to resting UES pressure of muscle fibers of the inferior pharyngeal constrictor and proximal esophagus.

In all normal swallows UES pressure drops rapidly just before UES opening and transsphincteric flow (Fig. 5). In one-third of the subjects this initial drop in pressure was followed by an additional transient drop to subatmospheric pressures, as has been noted previ-

ously (8, 12, 25, 41). Whereas past studies have sometimes attributed this drop to an artifact associated with catheter motion, it has recently been argued from mechanical principles and physiological data analysis that the transition to subatmospheric drop corresponds closely to the instant at which the anterior-posterior walls of the UES separate and UES opening begins (22). Figure 2*A*, in particular, shows that just at the time of UES opening, as described by Hsieh (22), the sudden anterior motion of the cricoid cartilage by anterior traction forces generated by anterior hyoid motion causes a momentary drop to subatmospheric pressures over a segment 2 cm in length.

The findings in the present study reinforce the close association between the occurrence of an intrasphincteric subatmospheric pressure drop and the passage of the bolus head into the UES (Fig. 2) and the anterior excursion of the hyoid bone (Fig. 5). In fact, using a mathematical model of UES opening, Hsieh (22) predicted that the drop in subatmospheric pressures ends when the bolus head passes into the narrow UES segment, driving the pressure back toward atmospheric. This characteristic is verified in Fig. 2. When present, consistent with Hsieh's model (22), a subatmospheric pressure drop provides a nonradiological marker of UES opening.

REFERENCES

1. **Ali GN, Laundl TM, Wallace KL, Shaw DW, and Cook IJ.** Influence of mucosal receptors on the deglutitive regulation of pharyngeal and upper esophageal sphincter function. *Am J Physiol Gastrointest Liver Physiol* 267: G644–G649, 1994.

2. **Ali GN, Wallace KL, Laundl TM, Hunt DR, deCarle DJ, and Cook IJ.** Predictors of outcome following cricopharyngeal disruption for pharyngeal dysphagia. *Dysphagia* 12: 133–139, 1997.

3. **Ali GN, Wallace KL, Schwartz R, de Carle DJ, Zagami A, and Cook IJ.** Mechanisms of oral-pharyngeal dysphagia in patients with Parkinson's disease. *Gastroenterology* 110: 383–392, 1996.

4. **Asoh R and Goyal RK.** Manometry and electromyography of the upper esophageal sphincter in the opossum. *Gastroenterology* 74: 514–520, 1978.

5. **Bonington A, Mahon M, and Whitmore I.** A histological and histochemical study of the cricopharyngeus muscle in man. *J Anat* 156: 27–37, 1988.

6. **Brasseur J and Dodds W.** Interpretation of intraluminal manometric measurements in terms of swallowing mechanics. *Dysphagia* 6: 100–119, 1991.

7. **Castell J, Dalton C, and Castell D.** Pharyngeal and upper esophageal sphincter manometry in humans. *Am J Physiol Gastrointest Liver Physiol* 258: G173–G178, 1990.

8. **Cerenko D, McConnel F, and Jackson R.** Quantitative assessment of pharyngeal bolus driving forces. *Otolaryngol Head Neck Surg* 100: 57–63, 1989.

9. **Clouse RE, Alrakawi A, and Staiano A.** Intersubject and interswallow variability in topography of esophageal motility. *Dig Dis Sci* 43: 1978–1985, 1998.

10. **Clouse RE and Staiano A.** Topography of normal and high-amplitude esophageal peristalsis. *Am J Physiol Gastrointest Liver Physiol* 265: G1098–G1107, 1993.

11. **Clouse RE, Staiano A, and Alrakawi A.** Topographic analysis of esophageal double-peaked waves. *Gastroenterology* 118: 469–476, 2000.

12. **Cook IJ, Dodds WJ, Dantas RO, Massey B, Kern MK, Lang IM, Brasseur JG, and Hogan WJ.** Opening mechanisms of the human upper esophageal sphincter. *Am J Physiol Gastrointest Liver Physiol* 257: G748–G759, 1989.

13. **Cook IJ, Gabb M, Panagopoulos V, Jamieson GG, Dodds WJ, Dent J, and Shearman DJ.** Pharyngeal (Zenker's) diverticulum is a disorder of upper esophageal sphincter opening. *Gastroenterology* 103: 1229–1235, 1992.

14. **Crowder M and Hand D.** *Analysis of Repeated Measures.* London: Chapman and Hall, 1991.

15. **Dantas RO, Cook IJ, Dodds WJ, Kern MK, Lang IM, and Brasseur JG.** Biomechanics of cricopharyngeal bars. *Gastroenterology* 99: 1269–1274, 1990.

16. **Dent J.** A new technique for continuous sphincter pressure measurement. *Gastroenterology* 71: 263–267, 1976.

17. **DiRe C, Shi G, and Kahrilas P.** UES pressure measured with a microsleeve: Going, going, . . . (Abstract). *Gastroenterology* 116: A4288, 1999.

18. **Dodds WJ, Hogan WJ, Lydon SB, Stewart ET, Stef JJ, and Arndorfer RC.** Quantitation of pharyngeal motor function in normal human subjects. *J Appl Physiol* 39: 692–696, 1975.

19. **Easterling C, Kern M, Nitschke T, Grande B, Kazandjian M, Dikeman K, Massey B, and Shaker R.** Restoration of oral feeding in 17 tube fed patients by the Shaker exercise (Abstract). *Dysphagia* 15: 105, 2000.

20. **Goyal RK, Martin SB, Shapiro J, and Spechler SJ.** The role of cricopharyngeus muscle in pharyngoesophageal disorders. *Dysphagia* 8: 252–258, 1993.

22. **Hsieh P-Y.** *Mechanical Function of the Upper Esophageal Sphincter During Opening and Transsphincteric Flow* (PhD thesis). University Park, PA: Pennsylvania State Univ., 1995.

23. **Indireshkumar K, Brasseur J, Faas H, Hebbard G, Kunz P, Dent J, Boesinger P, Feinle C, Fried M, Li M, and Schwizer W.** Relative contributions of "pressure pump" and "peristaltic pump" to slowed gastric emptying. *Am J Physiol Gastrointest Liver Physiol* 278: G604–G616, 2000.

24. **Isberg A, Nilsson ME, and Schiratzki H.** Movement of the upper esophageal sphincter and a manometric device during deglutition, a cineradiographic investigation. *Acta Radiol* 26: 381–388, 1985.

25. **Jacob P, Kahrilas P, Logemann J, Shah V, and Ha T.** Upper esophageal sphincter opening and modulation during swallowing. *Gastroenterology* 97: 1469–1478, 1989.

26. **Janiak P, Ghosh S, Thurmshirn M, Brasseur J, Fried M, Hebbard G, and Schwizer W.** Does high resolution manometry detect esophageal motility disorders more reliably than conventional manometry? (Abstract). *Gastroenterology* 118: A132, 2000.

27. **Kahrilas PJ, Dent J, Dodds WJ, Hogan WJ, and Arndorfer RC.** A method for continuous monitoring of upper esophageal sphincter pressure. *Dig Dis Sci* 32: 121–128, 1987.

28. **Kahrilas PJ, Dodds WJ, Dent J, Logemann JA, and Shaker R.** Upper esophageal sphincter function during deglutition. *Gastroenterology* 95: 52–62, 1988.

29. **Lang IM and Shaker R.** An update on the physiology of the components of the upper esophageal sphincter. *Dysphagia* 9: 229–232, 1994.

30. **Lang IM and Shaker R.** Anatomy and physiology of the upper esophageal sphincter. *Am J Med* 103: 50S–55S, 1997.

31. **Li M, Brasseur J, P Hsieh-Y, Nicosia M, Kern M, and Massey B.** A conversion methodology to analyse manometric pressure data in space-time (Abstract). *Gastroenterology* 106: A530, 1994.

32. **Li M, Brasseur J, Kern M, and Dodds W.** Viscosity measurements of barium sulfate mixtures for use in motility studies of the pharynx and esophagus. *Dysphagia* 7: 17–30, 1992.

33. **Maddock DJ and Gilbert RJ.** Quantitative relationship between liquid bolus flow and laryngeal closure during deglutition. *Am J Physiol Gastrointest Liver Physiol* 265: G704–G711, 1993.

34. **Mason RJ, Bremner CG, DeMeester TR, Crookes PF, Peters JH, Hagen JA, and DeMeester SR.** Pharyngeal swallowing disorders: selection for and outcome after myotomy. *Ann Surg* 228: 598–608, 1998.

35. **Nilsson ME, Isberg A, and Schiratzki H.** The location of the upper oesophageal sphincter and its behaviour during bolus propagation—a simultaneous cineradiographic and manometric investigation. *Clin Otolaryngol* 14: 61–65, 1989.

36. **Omari T, Bakewell M, Fraser R, Davidson G, and Dent J.** Intraluminal micromanometry: an evaluation of the dynamic performance of micro-extrusions and sleeve sensors. *Neurogastroenterol Motil* 8: 241–245, 1996.

37. **Orlowski J, Dodds W, Linehan J, Dent J, Hogan W, and Arndorfer R.** Requirements for accurate manometric recording of pharyngeal and esophageal peristaltic pressure waves. *Invest Radiol* 17: 567–572, 1982.

38. **Press WH, Teukolsky SA, Vetterling WT, and Flannery BP.** *Numerical Recipes in C* (2nd ed.). Cambridge, UK: Cambridge Univ. Press, 1992.

39. **Shaker R, Kern M, Bardan E, Taylor A, Stewart ET, Hoffmann RG, Arndorfer RC, Hofmann C, and Bonnevier J.** Augmentation of deglutitive upper esophageal sphincter opening in the elderly by exercise. *Am J Physiol Gastrointest Liver Physiol* 272: G1518–G1522, 1997.

40. **Shaw DW, Cook IJ, Jamieson GG, Gabb M, Simula ME, and Dent J.** Influence of surgery on deglutitive upper esophageal sphincter mechanics in Zenker's diverticulum. *Gut* 38: 806–811, 1996.

41. **Sokol EM, Heitmann P, Wolf BS, and Cohen BR.** Simultaneous cineradiographic and manometric study of the pharynx, hypopharynx, and cervical esophagus. *Gastroenterology* 51: 960–974, 1966.

42. **Warwick R and Williams PL.** *Gray's Anatomy* (36th ed.). Philadelphia, PA: Saunders, 1980.